Design of a Novel Dual Flux Modulation Machine with Consequent-Pole Spoke-Array Permanent Magnets in Both Stator and Rotor

Ziyi Liang, *Student Member, IEEE* ,Yuting Gao, *Member, IEEE*, Dawei Li, *Member, IEEE,* and Ronghai Qu, *Fellow, IEEE*
(Invited)

***Abstract*—In this paper, a novel dual flux modulation (DFM) machine with consequent-pole spoke-array permanent magnets (PMs) in both stator and rotor is proposed to achieve a larger torque density than regular flux modulation machines. The stator has two portions of PMs, one is set next to the stator slot with circumferential magnetization, and the other is inserted between the stator yoke and flux bridge with radial magnetization. The rotor has consequent-pole spoke-array PMs and alternative flux bridges. The proposed DFMPM machine can be regarded as the combination of the flux switching PM (FSPM) machine and vernier PM (VPM) machine. First, the structure and operational principle are introduced. Then, the proposed 12-stator-slot/10-rotor-tooth dual flux modulation permanent magnet (DFMPM) machine is compared with the FSPM machine and VPM machine in terms of flux lines distribution, back-electromotive force (EMF), cogging torque and average torque. Finally, the four proposed DFMPM machines are optimized for maximum average torque and minimum ripple torque considering the effects of split ratio, slot opening ratio, PM depth, PM angle and iron angle.**

***Index Terms*—Dual flux modulation (DFM), flux bridges, torque density, flux switching (FS), vernier.**

I. INTRODUCTION

DIRECT-drive machines have a great potential in low-speed high-torque applications, including wind power generator, electric vehicles, etc. However, the low-speed and high-torque characteristics always make direct-drive PM machines have heavy weight and large material consumption. Hence, high torque density PM machines have drawn a large attention and many novel topologies, such as vernier PM (VPM) machine[1], flux switching PM (FSPM) machine[2] and flux reversal PM (FRPM) machine[3] are proposed. Based on the magnetic gear effect [4] or flux modulation effect [5], VPM, FSPM and FRPM machines are divided to flux modulation permanent magnet (FMPM) machine family.

VPM machine was firstly proposed in 1995 [1], and the operational principle of VPM machine, i.e., the magnetic gear effect was introduced in [6]. Much outstanding work has been done on the design and analysis of new VPM topologies [7-11].

This article was submitted for review on 28, February, 2018.
This work was supported by National Natural Science Foundation of China (NSFC) under Project Number 51520105010 and 51607079.
Z. Liang, Y. Gao, D. Li, and R. Qu are with the State Key Laboratory of Advanced Electromagnetic Engineering and Technology, School of Electrical and Electronic Engineering, Huazhong University of Science and Technology, Wuhan 430074, China(*e-mail: gyt626890@gmail.com).

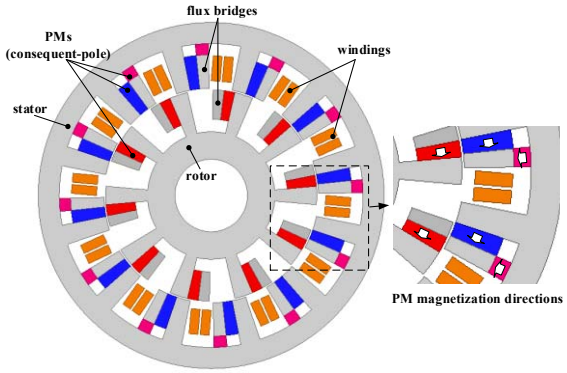

Fig. 1. Configuration of the proposed DFMPM machine

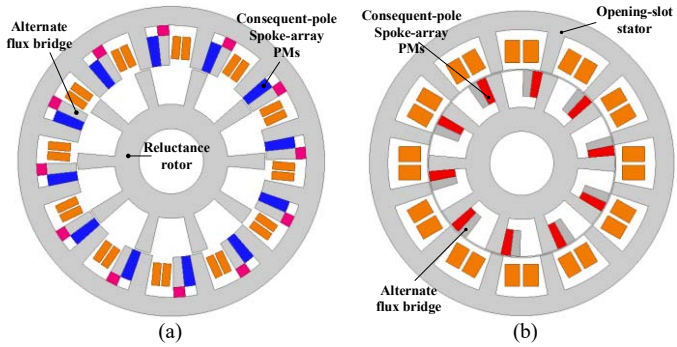

Fig. 2. Decomposition of the proposed DFMPM machine: (a) Machine I; (b) Machine II

These novel machines can be classified by a) different rotor topologies, i.e., surface mounted [7], Halbach-array type [8], spoke-array type [9] and double rotor [10]; b) different stator structures, such as split-tooth structure [11], hybrid-tooth structure [12] and double stator [13].

FSPM machine was firstly presented in 1955 [14], and it has several advantages [15], such as the simple rotor structure and high power density, which make it become the promising candidate for low-speed high-torque applications, like electric vehicle [16], linear servo system [17], fault tolerant [18] and so on. Many novel topologies including multi-tooth [19], E-core stator [20], C-core stator [21] and hybrid FSPM [22] were published to significantly reduce the magnet usage, while increase the torque density.

In order to improve the torque density of direct-drive machine, a novel flux modulation machine, which employs three portions of PMs, two on the stator and the other in the rotor, will be proposed in this paper. Two sets of PMs, which

are attached to the side-faces of stator slots and rotor teeth, respectively, are consequent-pole spoke-array PMs. Meanwhile, the alternative flux bridges are designed to reduce the flux barrier effect [23]. Besides, another set of PMs, which is inserted between the flux bridge and the stator yoke, is radially magnetized with the same polarity. The proposed machine can be identified as the combination of the FSPM machine and VPM machine. Hence, we name it as dual flux modulation permanent magnet machine with consequent-pole spoke-array PMs in both stator and rotor.

The organization of this paper is as follows. First, Section II will introduce the structure of the proposed DFMPM machine. Then, the operational principle of the DFMPM machine will be analyzed in Section III. Additionally, the proposed DFMPM machine will be compared to the optimized FSPM machine and VPM machine in terms of flux lines distribution, back-EMF, cogging torque and average torque by finite element analysis (FEA) in Section IV. Moreover, in Section V, the optimal design of some key parameters such as rotor tooth number, split ratio, opening ratio, PM depths and angles on the torque characteristics will be researched. Finally, some conclusions are drawn in Section VI.

II. Structure

Fig.1 shows the structure of the proposed DFMPM machine. The stator has two portions of PMs with different magnetization directions. As shown in Fig. 1, the magnets marked with blue color set near the stator slots with circumferential magnetization in the same polarity, and the PMs signed with pink color, which on the top of each flux bridge, are radially magnetized. The magnetization direction of the radial PMs is opposite with that of the pole leakage flux to reduce the flux leakage and increase the main flux. Meanwhile, the rotor has a consequent-pole structure with spoke-array PMs, which are circumferentially magnetized with the same polarity (either N or S). The alternate flux bridges next to rotor PMs are designed to weaken the flux barrier effect [23] and strengthen the flux modulation effect. Moreover, the consequent-pole spoke-array PMs in both stator and rotor are magnetized in the same direction. It can be seen that the configuration of armature winding is similar to that of conventional three-phase winding types including concentrated winding and distributed winding.

The proposed dual flux modulation machine can be regarded as overlay of two different machines: a consequent-pole FSPM machine with alternate flux bridges (Machine I) and a consequent-pole VPM machine taking iron flux bridges (Machine II), shown in Fig.2. The Machine I is made up of a stator having two sets of PMs with iron flux bridges and a reluctance rotor, which can be considered as the flux modulation machine with stationary excitation MMF. The Machine II is composed of the open-slot stator and consequent-pole spoke-array PM rotor with alternative flux bridges, which can be realized as the flux modulation machine with stationary flux modulator. Hence, the proposed machine works on dual flux modulation effect.

III. Operational Principle

The operational principle of the proposed DFMPM machine is based on the flux modulation principle. In order to make the magnetic fields created by PMs in both stator and rotor induce back-EMF in the same stator armature winding, the number of winding pole pair n_p, rotor tooth Z_r and stator slot Z_s should satisfy:

$$n_p = \{|Z_r \pm Z_s|; \frac{Z_s}{GCD(Z_s, n_p)} = 3k\} \qquad (1)$$
$$k = 1,2,3...$$

To illustrate the operational principle, the analytical method and 2-D FEA method are used. Before the analytical study, several assumptions are made as following:

- The stator iron and rotor iron are unsaturated.
- The fringing effect and the end effect are neglected.
- At the initial time, both the magnetomotive force (MMF) and permeance are set in the original point.
- High-order harmonics of PM MMF and air-gap permeance are neglected..

Based on the dual flux modulation effect, the PM MMF can be divided into two parts corresponding to Machine II and I.

$$\begin{aligned} F(\theta_s, t) &= F_R(\theta_{Rs}, t) + F_S(\theta_{Ss}, t) \\ &= F_R \cos(Z_r \theta_{Rs} - \omega t) \\ &+ F_S \cos(Z_s \theta_{Ss})] \end{aligned} \qquad (2)$$

where F_R is the PM MMF excited by the rotor PMs, F_S is the PM MMF created by the stator PMs, ω is the electrical velocity, θ_{Rs} and θ_{Ss} are the particular positions on the stator when two portions of PMs are worked separately. The air-gap permeance function can be calculated as:

$$\begin{aligned} \Lambda(\theta_s, t) = \frac{g}{\mu_0}&[\Lambda_{s0} - \Lambda_{s1} \cos(Z_s \theta_s)] \\ &\times [\Lambda_{r0} - \Lambda_{r1} \cos(Z_r \theta_s - \omega t)] \end{aligned} \qquad (3)$$

where Λ_s is the air-gap permeance function of slotted stator and Λ_r is the air-gap permeance function of slotted rotor.

Only considering the main working flux harmonics, the flux density can be expressed as:

$$\begin{aligned} B(\theta_s, t) &= F(\theta_s, t)\Lambda(\theta_s, t) \\ &= B_R(\theta_{Rs}, t) + B_S(\theta_{Ss}, t) \end{aligned} \qquad (4)$$

$$\begin{aligned} B_R(\theta_{Rs}, t) &= F_R \Lambda_{s0} \Lambda_{r0} \cdot \cos(Z_r \theta_{Rs} - \omega t) \\ &- \frac{1}{2} F_R \Lambda_{s1} \Lambda_{r0} \cdot \cos[(Z_s - Z_r)\theta_{Rs} + \omega t)] \\ &+ \frac{1}{2} F_R \Lambda_{s1} \Lambda_{r0} \cdot \cos[(Z_s + Z_r)\theta_{Rs} - \omega t)] \end{aligned} \qquad (5)$$

$$\begin{aligned} B_S(\theta_{Ss}, t) &= -\frac{1}{2} F_S \Lambda_{s0} \Lambda_{r1} \cdot \cos[(Z_s - Z_r)\theta_{Ss} + \omega t)] \\ &+ \frac{1}{2} F_S \Lambda_{s0} \Lambda_{r1} \cdot \cos[(Z_s + Z_r)\theta_{Ss} - \omega t)] \end{aligned}$$

where B_R is the air-gap flux density excited by the rotor PMs, B_S is the air-gap flux density created by the stator PMs.

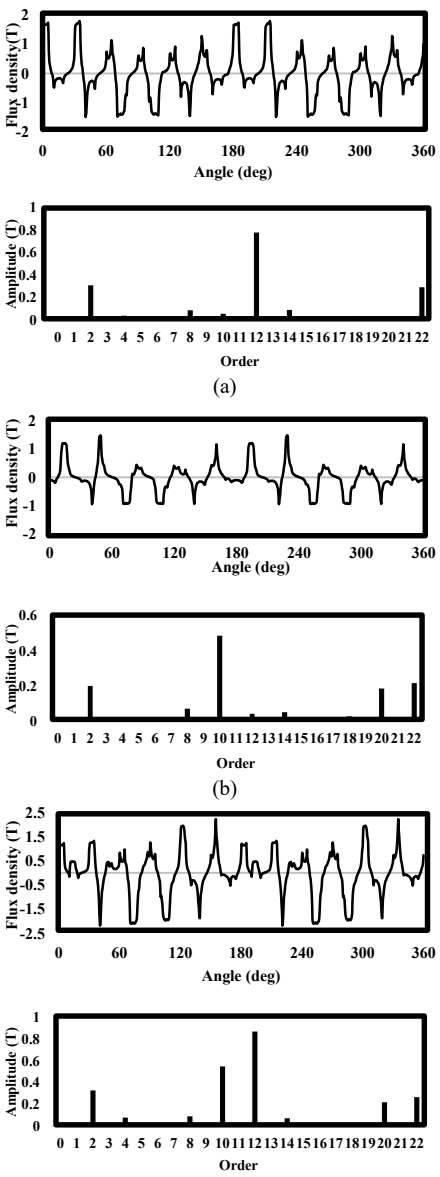

Fig. 3. Flux density waveform in air-gap and their FFT spectrum. (a) Excited by stator PMs (b) Excited by rotor PMs (c) Excited by stator and rotor PMs

To explain the operational principle of the dual flux modulation PM machine more clearly, a proposed DFMPM machine with 12-stator-slot /10-rotor-tooth is taken as an example. The Fig. 3 is obtained via FEA method. The magnetic field created by the PMs on the stator is illustrated in Fig.3 (a). The 2nd (Z_s-Z_r) pole pair air-gap flux density takes the largest contribution to the production of no-load back-EMF, while the 12th (Z_s) harmonic is static that not generates the back-EMF in the stator armature winding. As shown in Fig. 3. (b), the magnetic field excited by the PMs on the rotor is taken into account. It can be seen that the main flux density harmonics in the air-gap are the 2nd (Z_s-Z_r) and the 10th (Z_r) pole pairs, which produce by interaction of rotor PM MMF with stator air-gap permeance fundamental harmonic Λ_{s1} and constant component Λ_{s0}, respectively. The air-gap flux density of the proposed DFMPM machine is shown in Fig. 3 (c). The PM MMFs excited by stator and rotor PMs are 12th (Z_s) and 10th (Z_r). After the dual flux modulation effect, there are additional 2nd (Z_s-Z_r) and 22nd (Z_s+Z_r) pole pair flux density in the air-gap, and the 2nd pole pair air-gap flux density becomes the main working flux harmonic. According to the expressions (4) and (5), the results of air-gap flux density harmonics by FEA study match well with abovementioned analytical analysis.

IV. Performance Analysis

In this part, the electromagnetic performances including flux lines distribution, back-EMF, average torque, ripple torque etc. of the proposed DFMPM machine are assessed by using FEA method. The simulation is used by Ansoft Maxwell 15.0 transient analysis, and the air-gap region is separated to four-layer meshes. For further validation, three cases are modeled for comparative study: FSPM machine only with stator PMs (Machine I), VPM machine only with rotor PMs (Machine II) and the proposed DFMPM machine with both rotor PMs and stator PMs (Machine III). In order to ensure the fairness of the comparison, some main dimensions of the three FMPM machines are the same such as the stator outer diameter, stack length, rotation speed, armature winding configuration etc. as listed in Table I. The three FMPM machines have been optimized respectively.

TABLE I
MAIN DIMENSIONS OF THREE FLUX-MODULATION MACHINES

Parameter	Machine I	Machine II	Machine III
Stator outer diameter		124mm	
Stator inner diameter		81.84mm	
Stack length		120mm	
Airgap length		0.6mm	
Rotor inner diameter		26mm	
Series turns per phase		200	
PM material		N42SH	
Iron core material		35TW250	
Rotation speed		300rpm	
Rated current		5A	
PM volume	86.803cm^3	51.84cm^3	128.528 cm^3

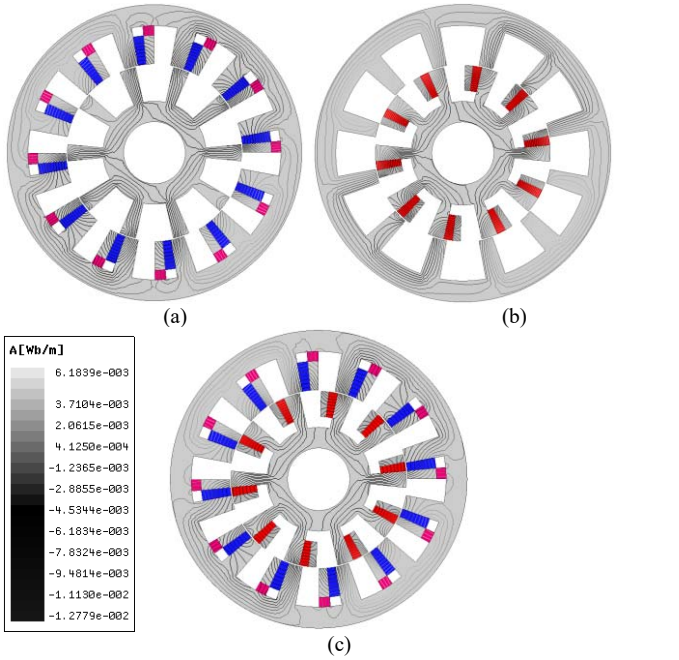

Fig. 4. Flux lines distribution of three machines: (a) Machine I; (b) Machine II; (c) Machine III

Fig. 4 illustrates the flux lines distribution plots of three machines. It can be noted that the pole pair number of the stator armature winding should be 2, which is agreed with the theoretical analysis on Eqn.1. (Z_s=12, Z_r=10, n_p=12-10=2). Moreover, the pole pair numbers of the Machine I and II are both 2. Therefore, a steady torque can be yielded by the interaction between the 2-pole-pair stator excitation field by the stator PMs, 2-pole-pair rotor excitation field by the rotor PMs and the 2-pole-pair armature field by the stator armature winding. Fig. 5 (a) shows the results of no-load back-EMF waveforms and the FFT spectrums of back-EMF waveforms are depicted in Fig. 5 (b). The fundamental amplitudes of back-EMF are72.54V, 65.05V and 123.52V for Machine I, II and III, respectively. It can be seen that the waveforms of the three PM machines are distorted a little, but there is no phase difference between the back-EMF waveforms excited by the stator PMs and rotor PMs.

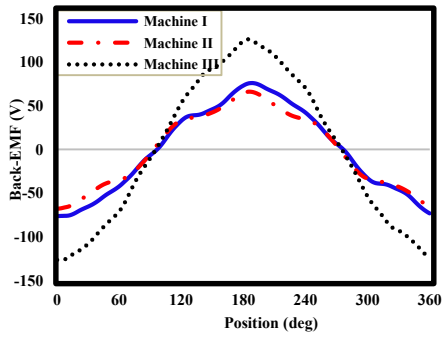

(a)

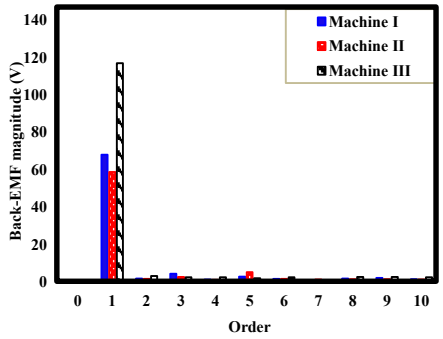

(b)

Fig. 5. Comparison of no-load back-EMF: (a) Waveforms; (b) FFT spectrum

Then, the torque capability is analyzed by injecting AC current into the stator armature winding. Based on the natural cooling and heat capacity, the current density of the three machines is selected as 120 A/cm, and the root-mean-square (rms) value of AC current is 5A. The cogging torques of the three flux modulation machines are illustrated in Fig.6. It can be seen that the Machine III exhibits the largest cogging torque, which the amplitude is about 2 Nm. Moreover, as shown in Fig.7 the average torques of three machine are 21.98 Nm, 20.12 Nm and 37.76 Nm for Machine I, II and III, respectively. It is obvious that the proposed DFMPM machine can achieve 71.8% higher and 87.8% higher torque than that of the Machine I and II, respectively.

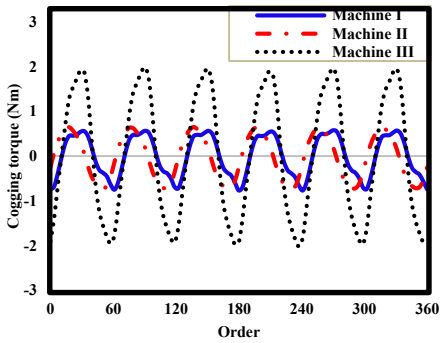

Fig. 6. Comparison of cogging torque.

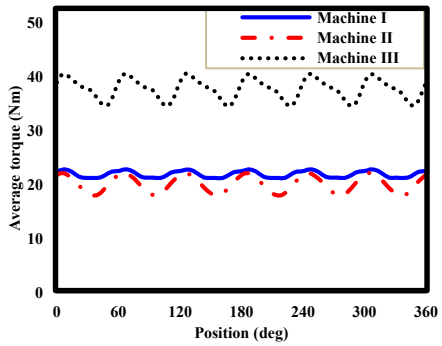

Fig. 7. Comparison of average torque.

TABLE II
MAIN PARAMETERS OF THE PROPOSED DFMPM MACHINE

Parameter	Value			
Stator slot number Z_s	12			
Rotor tooth number Z_r	10	11	13	14
Winding pole pair number P_n	2	1	1	2
Pole ratio PR	5	11	13	7
Stator outer diameter	124mm			
Stack length	120mm			
Airgap length	0.6mm			
Series turns per phase	200			
Split ratio	0.6			
PM material	N42SH			
Iron core material	35TW250			
Rotation speed	300rpm			
Winding pitch	1			
Rated current	5A			

PS: PR stands for the pole ratio that equals to the ratio of rotor tooth number Z_r to winding pole pair number n_p

V. OPTIMAL DESIGN

Based on the flux modulation effect, the stator slot and rotor tooth structures of the proposed machines are not only to provide the flux path, but also to modulate the magnetic circuit. Hence, the air-gap configuration significantly influences the key electromagnetic performances such as average torque and ripple torque. According to the analysis results in [6], 12-stator-slot FMPM machines with 10-, 11-, 13-, 14-rotor- tooth are found to produce relatively high torque density compared with other combination. Therefore, the above four combinations of DFMPM machines with the proposed topology are selected to optimize for relatively higher average torque and lower ripple torque. Firstly, the initial design parameters of four DFMPM machines are shown in Table II. It can be found that the stator outer diameter, winding pitch, rotation speed and materials of PMs are kept completely the same. Then, the influences of split

ratio, opening ratio, PM depth, PM angle and iron flux-bridge angle on the torque characteristics are researched by FEA method. Besides, the stator and rotor iron depths, which mean the lengths of the flux bridges, are equal to the corresponding PM depths.

A. Split Ratio Optimization

The split ratio is defined as the ratio of the stator inner diameter to stator outer diameter. When optimizing the split ratio, the stator slot opening ratio, rotor slot opening ratio, stator PM depth, rotor PM depth, stator PM angle, rotor PM angle, stator iron angle and rotor iron angle are kept as 0.76, 0.7, 10mm, 11mm, 5deg, 5deg, 5deg and 4deg, respectively. The ripple torque is considered as the ratio of peak-to-peak value of average torque waveform to average torque. Fig.8 (a) shows the effect of split ratio on average torque. It can be found that the optimal split ratio values for maximal average torque of the 10- and 14- rotor-tooth DFMPM machines are 0.68 and that of the 11- and 13- rotor-tooth DFMPM machines are 0.60 and 0.62, respectively. Due to the effect of the stator yoke saturation, the more winding pole pair and the less PR will make the stator yoke thickness smaller and the optimal split ratio larger. After that, the effect of split ratio on ripple torque is illustrated in Fig.8 (b). Author in [24] proved that the ripple torque relates to N_p, where N_p is given as:

$$N_p = LCM(Z_s, Z_r) \tag{6}$$

and LCM(Z_s, Z_r) stands for the least common multiple of stator slots and rotor teeth. The larger N_p, the lower ripple torque. The values of N_p in 10-, 11-, 13- and 14-rotor-tooth proposed DFMPM machines are 60, 132, 156 and 84. Therefore, the 12/11 and 12/13 proposed DFMPM machines have smaller ripple torque than that of 12/10 and 12/14 machines.

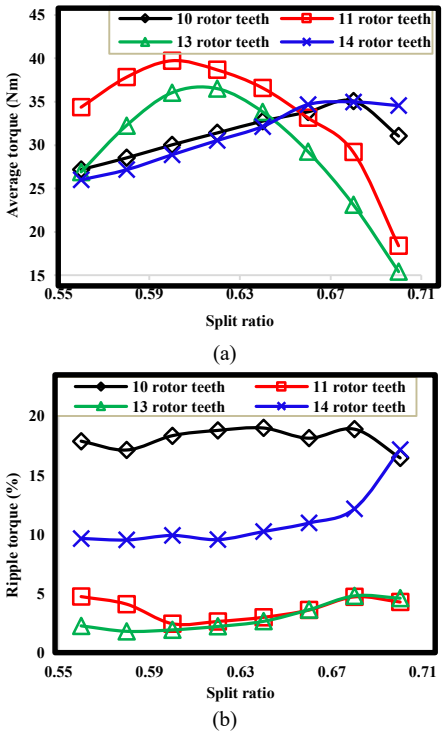

Fig. 8. Effect of split ratio on torque performances: (a) Average torque; (b) Ripple torque.

B. Slot Opening Ratio Optimization

The slot opening ratio is defined as the ratio of the slot opening width to slot pitch. When optimizing the stator slot opening ratio, the split ratio is kept as its corresponding optimal value, and the rotor slot opening ratio, stator PM depth, rotor PM depth, stator PM angle, rotor PM angle, stator iron angle and rotor iron angle are chose as 0.7, 10mm, 11mm, 5deg, 5deg, 5deg and 4deg, respectively. Fig. 9 presents the influences of stator slot opening ratio on average torque and ripple torque. It can be found that the average torque increases with the stator slot opening ratio in the beginning, due to the stronger flux modulation effect. However, when crossing the optimal point of stator slot opening ratio, the torque density decreases while the stator slot opening width becomes wider and wider. The main reason is that a wider stator slot opening width will increase the equivalent air-gap length. Meanwhile, as the stator slot opening ratio increases, the ripple torque decreases at first, and then it grows up. Additionally, a small stator slot opening ratio could bring the difficulty of stator winding arrangement. Hence, the optimal stator slot opening ratios for maximal torque and minimum ripple torque of 10-, 11-, 13- and 14-rotor-tooth DFMPM machines are 0.68, 0.7, 0.72 and 0.72.

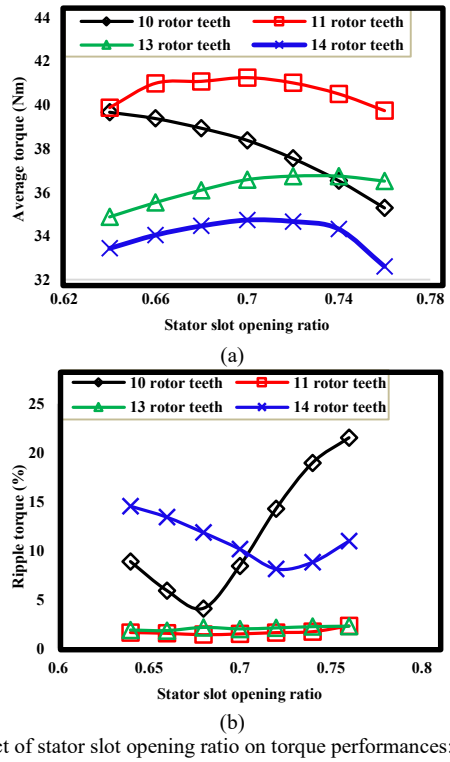

Fig.9. Effect of stator slot opening ratio on torque performances: (a) Average torque; (b) Ripple torque.

Then, the effect of the rotor slot opening ratio on torque characteristic is shown in Fig. 10. When optimizing the rotor slot opening ratio, the split ratio and stator slot opening ratio are kept as their corresponding optimal values, and the stator PM depth, rotor PM depth, stator PM angle, rotor PM angle, stator iron angle and rotor iron angle of those four DFMPM machines are selected as 10mm, 11mm, 5deg, 5deg, 5deg and 4deg, respectively. It is interesting to find that as the rotor slot opening ratio increases, the average torque gets larger initially due to the stronger modulation effect of rotor teeth, but it decreases

afterwards mainly because the rotor teeth are saturated. Furthermore, the lowest ripple torque of 12/10 and 12/14 proposed DFMPM machines is obtained when the rotor slot opening ratio is around 0.69, while that of the 12/11 and 12/13 proposed DFMPM machines does not change dramatically. Therefore, taking both average torque and ripple torque into consideration, the rotor slot opening ratios of 10-, 11-, 13-, and 14-rotor-tooth proposed DFMPM machines are 0.69, 0.72, 0.69 and 0.66, respectively.

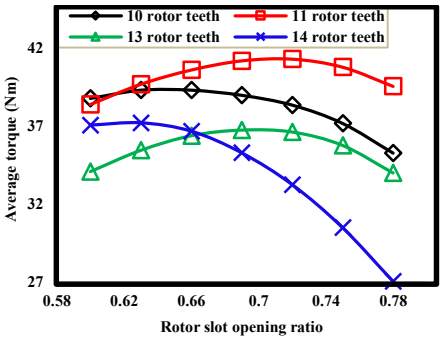

(a)

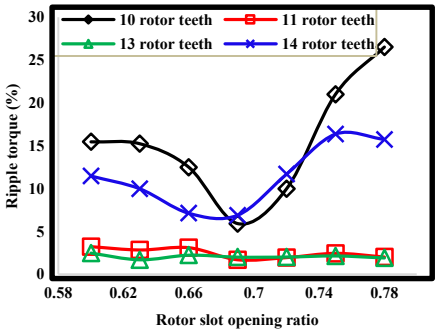

(b)

Fig.10. Effect of rotor opening ratio on torque performances: (a) Average torque; (b) Ripple torque.

C. *PM Depth and PM Angle Optimization*

The effects of both stator PM depth and rotor PM depth on average torque and ripple torque are illustrated in Fig. 11 and Fig. 12. When optimizing the PM depth, the split ratio and slot opening ratio are kept as their corresponding optimal values, and the stator PM angle, rotor PM angle, stator iron angle and rotor iron angle of four proposed DFMPM machines are selected as 5deg, 5deg, 5deg and 4deg, respectively. It can be seen that as the PM depth becomes larger and larger, the torque density gets higher in the beginning, but when the PM depth keeps rising, the torque density gets smaller as a result. This is because a deeper magnet not only produces a bigger PM MMF and a larger main flux, which increases the average torque, but also increases the saturation effect at the bottom of the stator slot and rotor tooth, which reduces the torque density. Then, the variations of ripple torque with the stator PM depth and rotor PM depth are depicted in Fig.11 (b) and Fig.12 (b). It shows that the ripple torque just changes a little with the increase of the PM depth. To take a comprehensive consideration, the optimal stator PM depth for the best torque performance of the four DFMPM machines is around 10.5mm to 11mm, and the optimal rotor PM depth is about 9.5mm to 10.5mm.

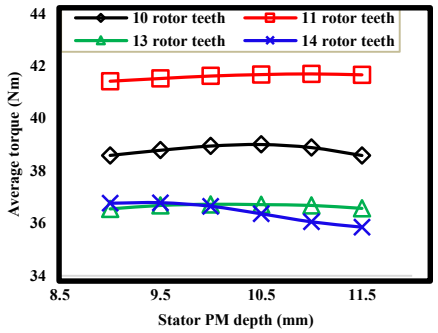

(a)

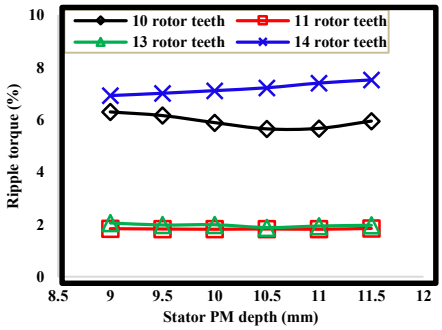

(b)

Fig.11. Effect of stator PM depth on torque performances: (a) Average torque. (b) Ripple torque.

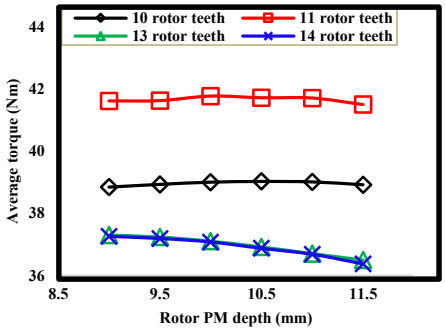

(a)

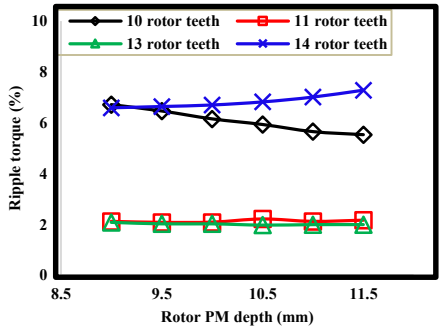

(b)

Fig.12. Effect of rotor PM depth on torque performances: (a) Average torque. (b) Ripple torque.

Another significant parameter of the magnets is the PM angle in circumferentially direction, whose effect on the average torque is revealed in Fig.13 (a) and Fig.14 (a). When optimizing the PM angle, the split ratio, slot opening ratio and PM depth are kept as their corresponding optimal values, and the stator iron angle and rotor iron angle of the four proposed DFMPM machines are chose as 5deg and 4deg, respectively. For the stator PM angle, the average torque monotonically increases with the PM width since a larger stator PM angle will generate

a higher PM MMF magnitude. However, with the considerations of the material cost and stator armature winding installation, the stator PM angle cannot be too large. Then, for the rotor PM angle, the average torque initially goes up with PM width, since the field excitation increases the magnet MMF value, and it reaches the maximum, while decreases as the saturation effect of the rotor tooth. Moreover, the effects of PM angle on ripple torque are shown in Fig.13 (b) and Fig.14 (b). It can be found that the ripple torques achieve their minimum values when the average torques obtain their corresponding maximum values.

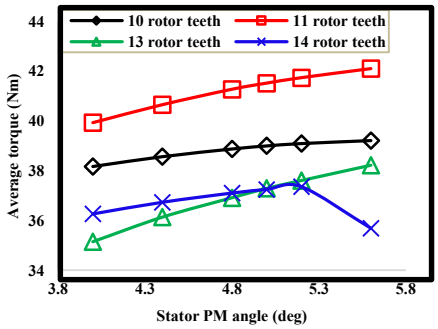

(a)

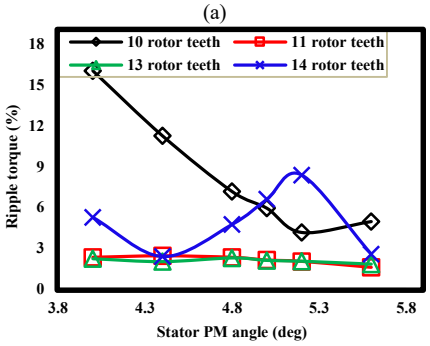

(b)

Fig.13. Effect of stator PM angle on torque performances: (a) Average torque; (b) Ripple torque.

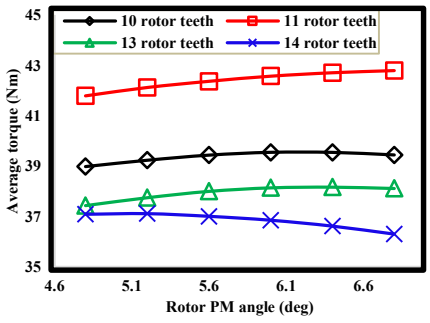

(a)

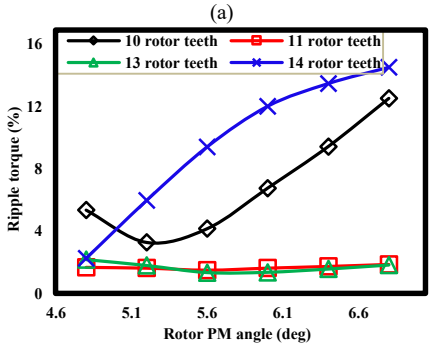

(b)

Fig.14. Effect of rotor PM angle on torque performances: (a) Average torque; (b) Ripple torque.

D. Iron Angle Optimization

The iron angle is defined as the angle of iron flux bridge in circumferentially direction. Fig. 15 and Fig. 16 analyze the influences of iron angle on average torque and ripple torque. When optimizing the iron angle, the split ratio, slot opening ratio PM depth and PM angle are kept as their corresponding optimal values. It can be noted that the average torques of 10-, 11-, 13- and 14-rotor-tooth DFMPM machines have the maximal values when stator iron angles are kept as 5deg, 4.6deg, 3.8deg and 4.2deg, respectively. However, when the rotor iron angle becomes higher, the average torque monotonically decreases due to the increase of the flux leakage and the reduction of the main flux. In order to facilitate the installation of the flux bridges, the rotor iron angle cannot be set too small. Therefore, the optimal rotor iron angle of four proposed DFMPM machines is 3 deg.

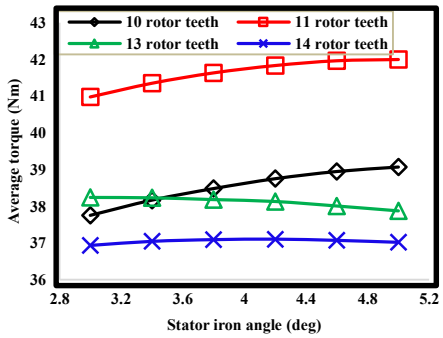

(a)

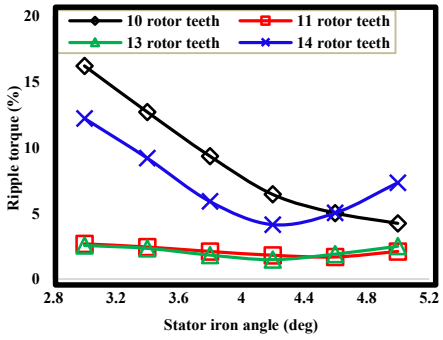

(b)

Fig.15. Effect of stator iron angle on torque performances: (a) Average torque; (b) Ripple torque.

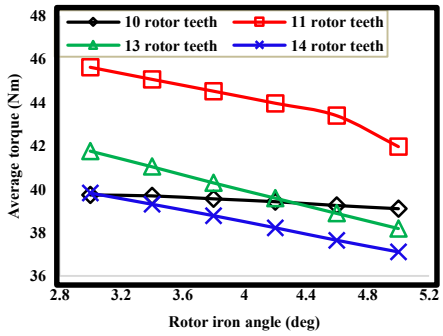

(a)

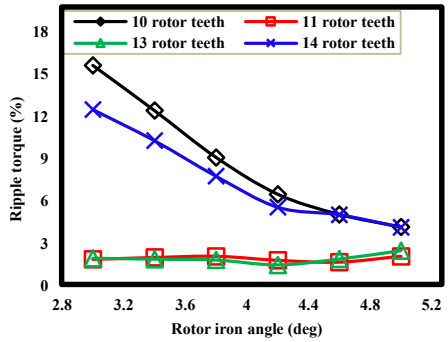

(b)

Fig.16. Effect of rotor iron angle on torque performances: (a) Average torque; (b) Ripple torque.

VI. Conclusion

In this paper, a novel dual flux modulation machine with consequent-pole spoke-array permanent magnets in both stator and rotor is proposed and analyzed. Based on the dual flux modulation effect, the analytical method and FEA method are used to investigate the working flux density harmonics of the proposed DFMPM machine. Furthermore, through comparing to a FSPM machine and a VPM machine, it is found that the proposed DFMPM machine can obtain more than 70% higher torque. Additionally, the effects of design parameters including rotor slot number, split ratio, slot opening ratio, PM depth, PM angle and iron angle on the torque characteristics have been researched. It can be seen that 11-rotor-tooth DFMPM machine exhibits larger torque than others, while the 13-rotor-tooth DFMPM machine has the lowest ripple torque.

References

[1] A. Ishizaki, T. Tanaka, K. Takasaki and S. Nishikata, "Theory and optimum design of PM Vernier motor," *1995 Seventh International Conference on Electrical Machines and Drives (Conf. Publ. No. 412)*, Durham, 1995, pp. 208-212.

[2] Z. Q. Zhu and J. T. Chen, "Advanced Flux-Switching Permanent Magnet Brushless Machines," in *IEEE Transactions on Magnetics*, vol. 46, no. 6, pp. 1447-1453, June 2010.

[3] Y. Gao, R. Qu, D. Li, J. Li and L. Wu, "Design of Three-Phase Flux-Reversal Machines With Fractional-Slot Windings," in *IEEE Transactions on Industry Applications*, vol. 52, no. 4, pp. 2856-2864, July-Aug. 2016.

[4] K. Atallah and D. Howe, "A novel high-performance magnetic gear," in *IEEE Transactions on Magnetics*, vol. 37, no. 4, pp. 2844-2846, Jul 2001..

[5] D. Li, R. Qu and J. Li, "Topologies and analysis of flux-modulation machines," *2015 IEEE Energy Conversion Congress and Exposition (ECCE)*, Montreal, QC, 2015, pp. 2153-2160.

[6] A. Toba and T. A. Lipo, "Generic torque-maximizing design methodology of surface permanent-magnet vernier machine," in *IEEE Transactions on Industry Applications*, vol. 36, no. 6, pp. 1539-1546, Nov/Dec 2000.

[7] J. Li, K. T. Chau, J. Z. Jiang, C. Liu and W. Li, "A New Efficient Permanent-Magnet Vernier Machine for Wind Power Generation," in *IEEE Transactions on Magnetics*, vol. 46, no. 6, pp. 1475-1478, June 2010.

[8] D. Li, R. Qu and Z. Zhu, "Comparison of Halbach and Dual-Side Vernier Permanent Magnet Machines," in *IEEE Transactions on Magnetics*, vol. 50, no. 2, pp. 801-804, Feb. 2014.

[9] B. Kim and T. A. Lipo, "Analysis of a PM Vernier Motor With Spoke Structure," in *IEEE Transactions on Industry Applications*, vol. 52, no. 1, pp. 217-225, Jan.-Feb. 2016.

[10] T. Zou, D. Li, R. Qu, J. Li and D. Jiang, "Analysis of a Dual-Rotor, Toroidal-Winding, Axial-Flux Vernier Permanent Magnet Machine," in *IEEE Transactions on Industry Applications*, vol. 53, no. 3, pp. 1920-1930, May-June 2017.

[11] T. Zou, D. Li, R. Qu, D. Jiang and J. Li, "Advanced High Torque Density PM Vernier Machine With Multiple Working Harmonics," in *IEEE Transactions on Industry Applications*, vol. 53, no. 6, pp. 5295-5304, Nov.-Dec. 2017.

[12] L. Xu, G. Liu, W. Zhao, X. Yang and R. Cheng, "Hybrid Stator Design of Fault-Tolerant Permanent-Magnet Vernier Machines for Direct-Drive Applications," in *IEEE Transactions on Industrial Electronics*, vol. 64, no. 1, pp. 179-190, Jan. 2017.

[13] Y. Gao, R. Qu, D. Li, H. Fang, J. Li and W. Kong, "A Novel Dual-Stator Vernier Permanent Magnet Machine," in *IEEE Transactions on Magnetics*, vol. 53, no. 11, pp. 1-5, Nov. 2017.

[14] S. E. Rauch and L. J. Johnson, "Design principles of flux-switching alternators," *AIEE Trans.*, vol. 74, pt. III, no. 3, pp. 1261–1268, Jan. 1955.

[15] D. Li, R. Qu, J. Li, "Synthesis of flux switching permanent magnet machine," *IEEE Trans. Energy Convers*., vol. 31, no. 1, pp. 106–117, 2016.

[16] Z. Q. Zhu and D. Howe, "Electrical Machines and Drives for Electric, Hybrid, and Fuel Cell Vehicles," in *Proceedings of the IEEE*, vol. 95, no. 4, pp. 746-765, April 2007.

[17] R. Cao, M. Cheng, C. Mi, W. Hua, X. Wang and W. Zhao, "Modeling of a Complementary and Modular Linear Flux-Switching Permanent Magnet Motor for Urban Rail Transit Applications," in *IEEE Transactions on Energy Conversion*, vol. 27, no. 2, pp. 489-497, June 2012.

[18] T. Raminosoa, C. Gerada and M. Galea, "Design Considerations for a Fault-Tolerant Flux-Switching Permanent-Magnet Machine," in IEEE Transactions on Industrial Electronics, vol. 58, no. 7, pp. 2818-2825, July 2011.

[19] J. T. Chen, Z. Q. Zhu and D. Howe, "Stator and Rotor Pole Combinations for Multi-Tooth Flux-Switching Permanent-Magnet Brushless AC Machines," in *IEEE Transactions on Magnetics*, vol. 44, no. 12, pp. 4659-4667, Dec. 2008.

[20] J. Chen, Z. Zhu, S. Iwasaki, and R. P. Deodhar, "A novel E-core switched flux PM brushless AC machine," *IEEE Trans. Ind. Appl.*, vol. 47, no. 3, pp. 1273–1282, May/Jun. 2011

[21] J. Chen, Z. Zhu, S. Iwasaki, and R. Deodhar, "Influence of slot opening on optimal stator and rotor pole combination and electromagnetic performance of switched-flux PM brushless AC machines," *IEEE Trans. Ind. Appl.*, vol. 47, no. 4, pp. 1681–1691, Jul./Aug. 2011.

[22] H. Hua, Z. Q. Zhu, "Novel partitioned stator hybrid excited switched flux machines," *IEEE Trans. Energy Convers*., vol. 32, no. 2, pp. 495-504, Jun. 2017.

[23] T. Zou, R. Qu, D. Li and D. Jiang, "Flux barrier effect of spoke-array magnets in flux-modulation machines," *2016 IEEE Conference on Electromagnetic Field Computation (CEFC)*, Miami, FL, 2016, pp. 1-1.

[24] D. Li, R. Qu, J. Li, W. Xu and L. Wu, "Synthesis of Flux Switching Permanent Magnet Machines," in *IEEE Transactions on Energy Conversion*, vol. 31, no. 1, pp. 106-117, March 2016.

Ziyi Liang (S'16) was born in China. She received the B.Eng. degree in electrical engineering from Huazhong University of Science and Technology, Wuhan, China, in 2017.She is currently working toward the Ph.D. degree in the same university now.

Her research interests include the design and analysis of novel permanent-magnet machines.

Yuting Gao (S'13-M'17) was born in China. She received the B.Eng. degree and Ph.D degree in electrical engineering from Huazhong University of Science and Technology, Wuhan, China, in 2012 and 2017, respectively. She is a postdoc in the same university now.

Her research interests include the design and analysis of novel permanent-magnet and superconducting synchronous machines.

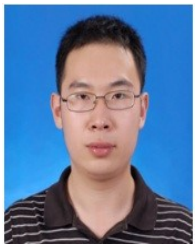

Dawei Li (S'12-M'15) was born in China. He received the B.E.E. degrees from Harbin Institute of Technology, Harbin, China, in 2010 and the Ph.D. degree in electrical engineering from Huazhong University of Science & Technology, in 2015. In Jul. 2015, he joined Huazhong University of Science &Technology, Wuhan, China. Dr. Li has authored over 60 published technical papers and is the holder of over 10 patents/patent applications. He was recipient of the 2016 Best Poster Presentation Award from the XXIIth International Conference on Electrical Machines (ICEM 2016), and Hubei Province Excellent Doctoral Dissertation (2016), China. His research areas include the design and analysis of flux-modulation permanent-magnet brushless machines.

Ronghai Qu (S'01–M'02–SM'05-F'18) was born in China. He received the B.E.E. and M.S.E.E. degrees from Tsinghua University, Beijing, China, in 1993 and 1996, respectively, and the Ph.D. degree in electrical engineering from the University of Wisconsin-Madison, in 2002.

In 1998, he joined the Wisconsin Electric Machines and Power Electronics Consortiums as Research Assistant. He became a Senior Electrical Engineer with Northland, a Scott Fetzer Company, NY in 2002. Since 2003, he had been with the General Electric (GE) Global Research Center, Niskayuna, NY, as a Senior Electrical Engineer with the Electrical Machines and Drives Laboratory. He has authored over 120 published technical papers and is the holder of over 50 patents/patent applications. From 2010, he has been a professor with Huazhong University of Science &Technology, Wuhan, China.

Prof. Qu is a full member of Sigma Xi. He has been the recipient of several awards from GE Global Research Center since 2003, including the Technical Achievement and Management Awards. He also is the recipient of the 2003 and 2005 Best Paper Awards, third prize, from the Electric Machines Committee of the IEEE Industry Applications Society at the 2002 and 2004 IAS Annual Meeting, respectively.